Electronic Supplementary Material (ESI) for Dalton Transactions.
This journal is © The Royal Society of Chemistry 2018

Supporting Information

Bright green-to-yellow emitting Cu(I) complexes based on bis(2-pyridyl)phosphine oxides: synthesis, structure and effective thermally activated-delayed fluorescence

Alexander V. Artem'ev,*[a] Maxim R. Ryzhikov,[a,b] Ilya V. Taidakov,[c,d] Mariana I. Rakhmanova,[a] Evgenia A. Varaksina,[c] Irina Yu. Bagryanskaya,[b,e] Svetlana F. Malysheva,[f] Nataliya A. Belogorlova[f]

[a] *Nikolaev Institute of Inorganic Chemistry, Siberian Branch of Russian Academy of Sciences, 3, Akad. Lavrentiev Ave., Novosibirsk 630090, Russian Federation*
[b] *Novosibirsk State University, (National Research University), Department of Natural Sciences, 2, Pirogova Str., Novosibirsk 630090, Russian Federation*
[c] *P. N. Lebedev Institute of Physics, Russian Academy of Sciences, 119991 Moscow, Russian Federation*
[d] *Dmitry Mendeleev University of Chemical Technology of Russia, Miusskaya sq. 9, 125047 Moscow, Russian Federation*
[e] *N. N. Vorozhtsov Novosibirsk Institute of Organic Chemistry, Siberian Branch of Russian Academy of Sciences, 9, Akad. Lavrentiev Ave., Novosibirsk 630090, Russian Federation*
[f] *A. E. Favorsky Irkutsk Institute of Chemistry, Siberian Branch of the Russian Academy of Sciences, 1 Favorsky Str., 664033 Irkutsk, Russian Federation*

*Author for correspondence: chemisufarm@yandex.ru (Alexander V. Artem'ev)

Table of Contents

X-Ray crystallography

Table S1. Data collection and refinement parameters for **2**–**7**.

Compound	**2**	**3**·2/3MeCN	**4**	**5**	**6**	**7**
CCDC number	1550541	1550542	1550543	1577810	1550544	1550545
Empirical formula	$C_{24}H_{26}Cu_2I_2N_4O_2P_2$	$C_{39.33}H_{56}Cu_2I_2N_{4.67}O_2P_2$	$C_{34}H_{30}Cu_2I_2N_4O_2P_2$	$C_{42}H_{34}Cu_2I_2N_4O_2P_2$	$C_{24}H_{22}Cu_2N_6O_2P_2S_2$	$C_{30}H_{34}Cu_2N_6O_2P_2S_2$
Formula mass [g/mol]	845.31	1069.04	969.44	1069.55	679.62	763.77
Space group	C2/c	P-1	C2/c	P-1	P-1	P-1
a [Å]	8.6569(3)	9.9811(4)	22.6984(7)	12.8420(9)	8.4316(4)	8.8655(10)
b [Å]	15.0992(5)	18.1601(8)	13.3472(4)	19.1700(12)	8.5325(4)	14.2395(16)
c [Å]	21.8930(8)	19.7982(9)	23.1883(6)	20.1670(13)	11.4693(6)	14.5066(16)
α [°]	90.00	71.782(2)	90.00	111.493(3)	74.268(2)	109.975(5)
β [°]	92.3170(10)	80.077(2)	90.8620(10)	94.250(3)	71.999(2)	90.384(5)
γ [°]	90.00	84.603(2)	90.00	108.188(3)	62.187(2)	103.193(5)
V [Å^3]	2859.34(17)	3354.6(3)	7024.3(4)	4287.8(5)	686.14(6)	1668.5(3)
Z	4	3	8	4	1	2
$D_{calcd.}$ [g·cm^{-3}]	1.964	1.588	1.833	1.657	1.645	1.520
μ [mm^{-1}]	3.788	2.440	3.097	2.546	1.853	1.533
Temperature [K]	296(2)	200(2)	200(2)	296(2)	296(2)	296(2)
Reflections collected	17174	29117	66274	62633	12135	18525
Independent reflections	3293 [R_{int} = 0.0448]	11792 [R_{int} = 0.0317]	9742 [R_{int} = 0.0432]	14604 [R_{int} = 0.0553]	3615 [R_{int} = 0.0295]	5640 [R_{int} = 0.0475]
R_1, wR_2 [$I > 2\sigma(I)$]	0.0256, 0.0652	0.0750, 0.1820	0.0259, 0.0595	0.0873, 0.1821	0.0269, 0.0755	0.0834, 0.1904
R_1, wR_2 (all data)	0.0291, 0.0767	0.1018, 0.1986	0.0358, 0.0645	0.1673, 0.2381	0.0309, 0.0787	0.1384, 0.2095
Goodness of fit	1.145	1.089	1.032	1.046	1.077	1.066
Largest diff peak and hole [e/Å^3]	1.10 and -0.79	2.56 and -2.13	1.22 and -1.03	2.91 and -2.12	0.40 and -0.38	1.88 and -0.60

Table S2. The structures of the three independent molecules in **3**·2/3MeCN and their selected bond lengths [Å] and angles [deg].

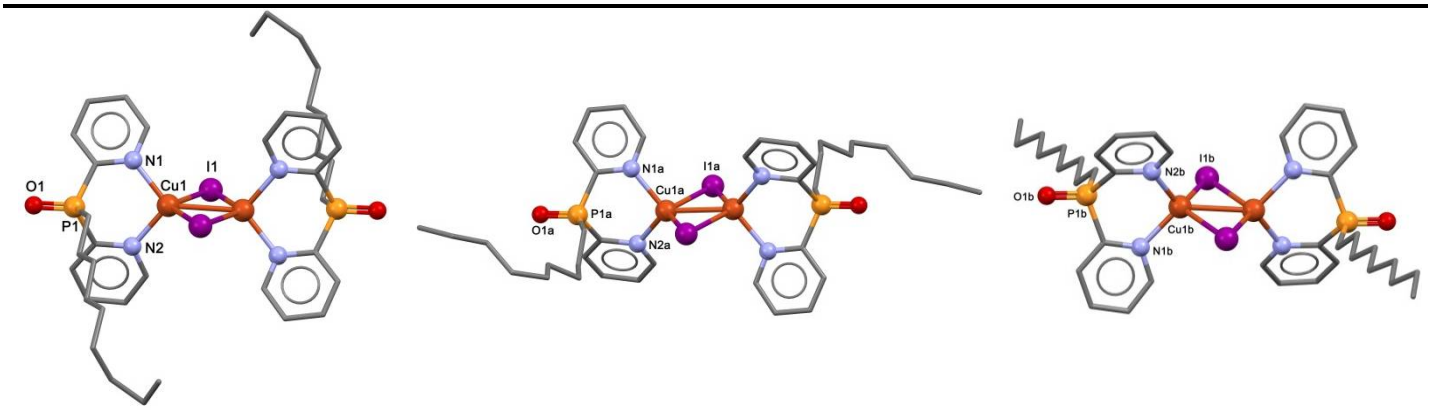

Cu–Cu	2.7187(19)	**Cu–Cu**	2.623(2)	**Cu–Cu**	2.6913(19)
Cu–I	2.6816(13)	**Cu–I**	2.6639(16)	**Cu–I**	2.5651(13)
Cu–I'	2.5797(13)	**Cu–I'**	2.5582(15)	**Cu–I'**	2.6697(14)
Cu–N^1	2.077(7)	**Cu–N^1**	2.098(10)	**Cu–N^1**	2.079(7)
Cu–N^2	2.088(7)	**Cu–N^2**	2.5583(15)	**Cu–N^2**	2.070(8)
I–Cu–I	117.81(4)	**I–Cu–I**	119.74(5)	**I–Cu–I**	118.16(4)
Cu–I–Cu	62.19(4)	**Cu–I–Cu**	60.27(5)	**Cu–I–Cu**	61.84(4)
N^1–Cu–N^2	100.4(3)	**N^1–Cu–N^2**	100.3(4)	**N^1–Cu–N^2**	101.8(3)
I–Cu–I–Cu	0.0	**I–Cu–I–Cu**	0.0	**I–Cu–I–Cu**	0.0

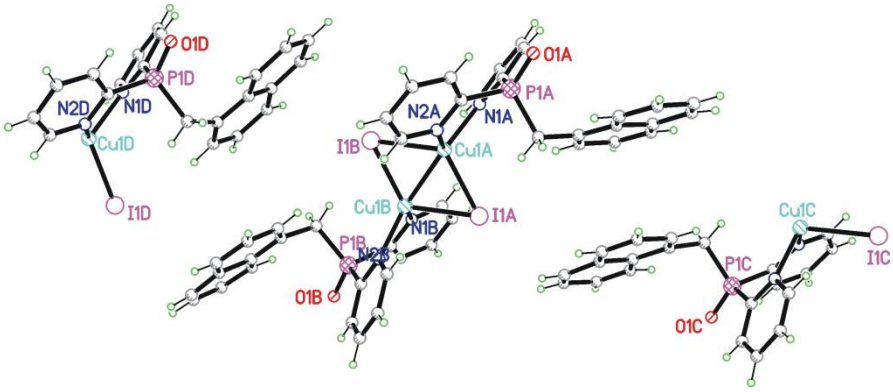

Figure S1. The structure of asymmetric unit of **5**.

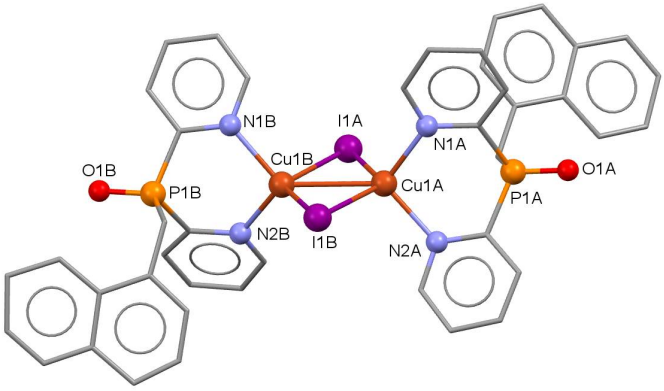

Figure S2. Molecular structure of **5** (the H atoms are omitted for clarity). Selected bond lengths [Å]: Cu(1A)–Cu(1B) 2.7444(19), Cu(1A)–I(1A) 2.5828(17), Cu(1A)–I(1B) 2.6573(18), Cu(1B)–I(1A) 2.6784(18), Cu(1B)–I(1B) 2.5660(17), Cu(1A)–N(1A) 2.090(10), Cu(1A)–N(2A) 2.097(11), Cu(1B)–N(2B) 2.079(10), Cu(1B)–N(1B) 2.088(11), P(1A)–O(1A) 1.490(8), P(1B)–O(1B) 1.481(9).

FT-IR spectra of 1-8

Figure S3. FT-IR spectrum of **{$Cu_2I_2[Py_2(Me)P{=}O]_2$}** (**1**) (*top*) and comparison (*bottom*) of experimental (black line) FT-IR spectrum of **{$Cu_2I_2[Py_2(Me)P{=}O]_2$}** (**1**) and theoretical IR spectra for 1-C_i (red line) and 1-C_2 (blue dashed line). Calculated spectra are scaled by 0.97 factor.

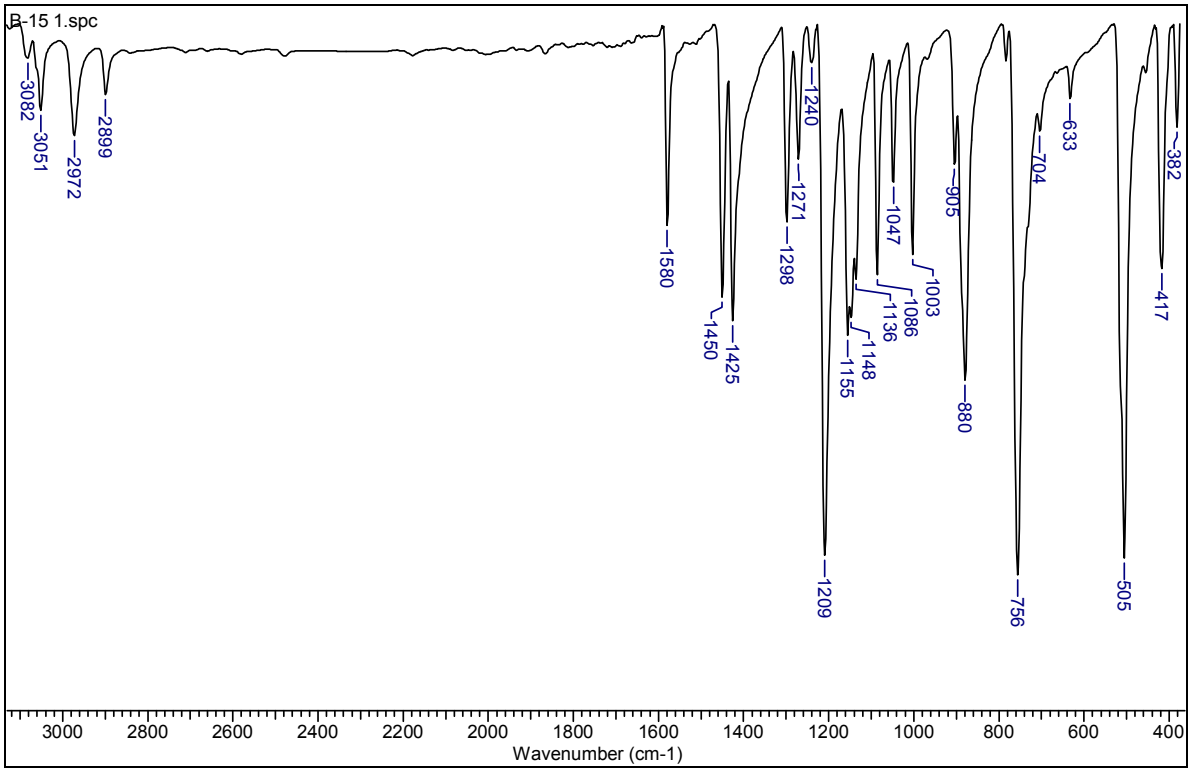

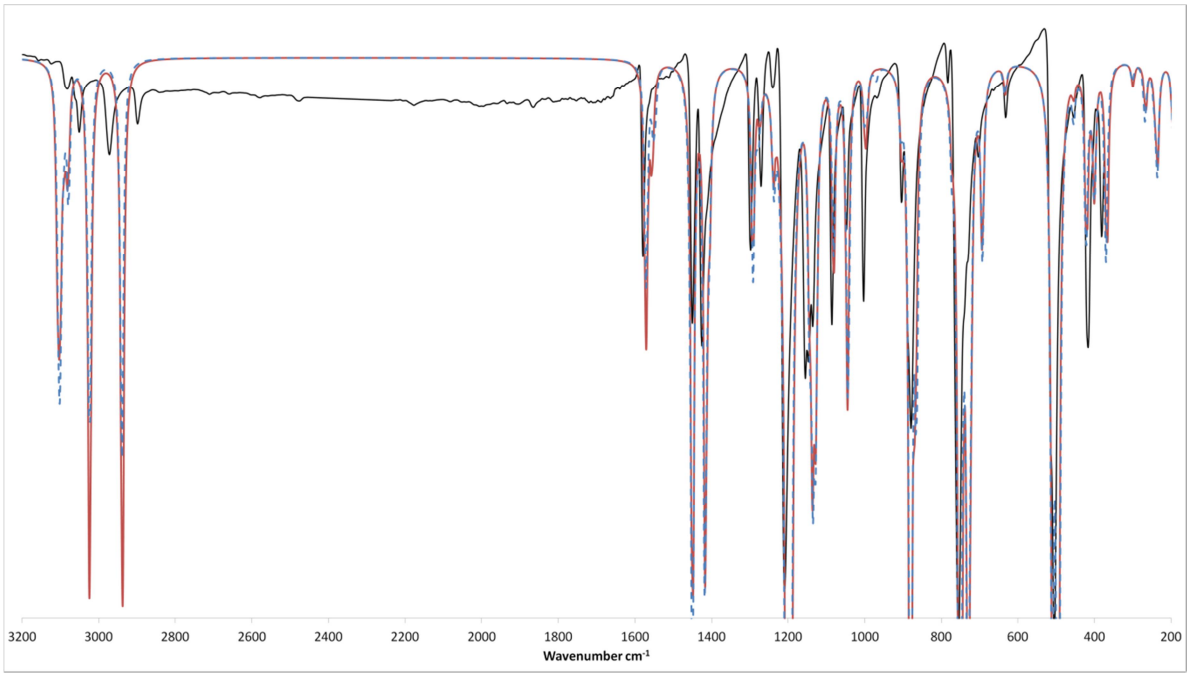

Figure S4. FT-IR spectrum of **{$Cu_2I_2[Py_2(Et)P{=}O]_2$}** (**2**).

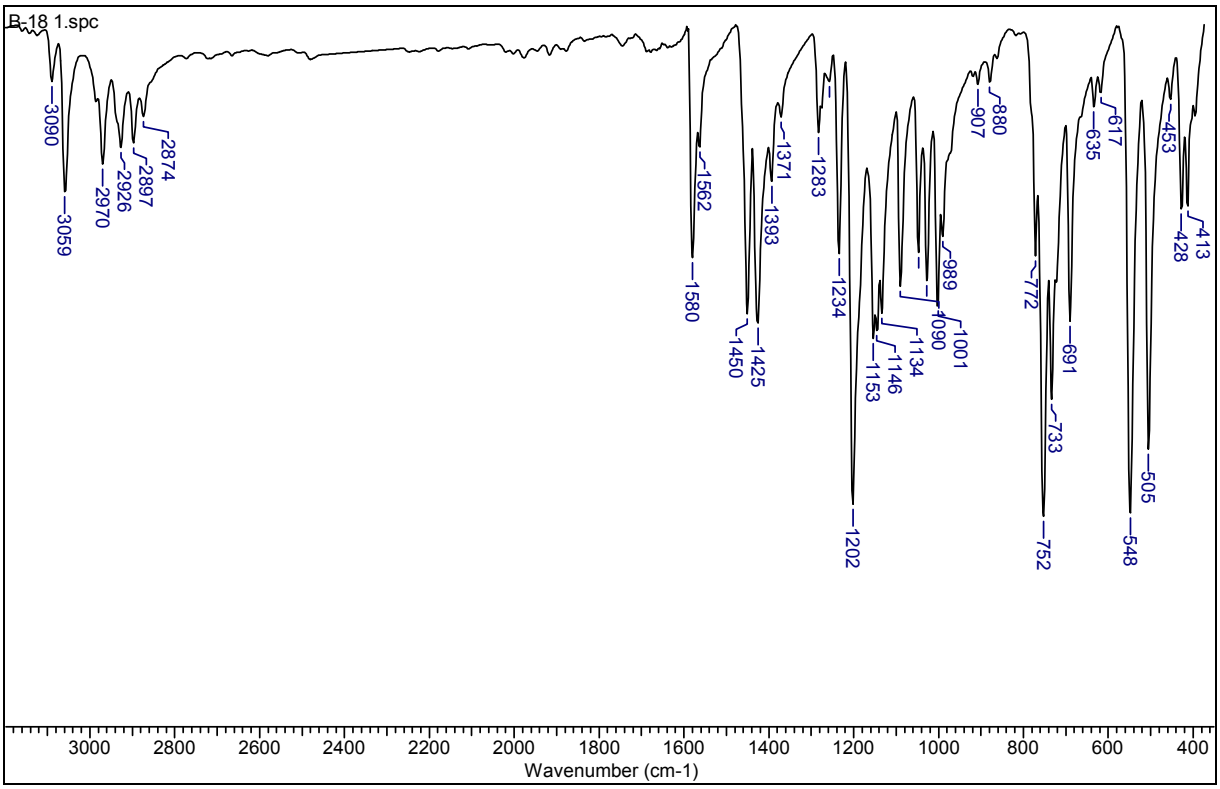

Figure S5. FT-IR spectrum of **{$Cu_2I_2[Py_2(n\text{-}C_9H_{19})P{=}O]_2$}** (**3**).

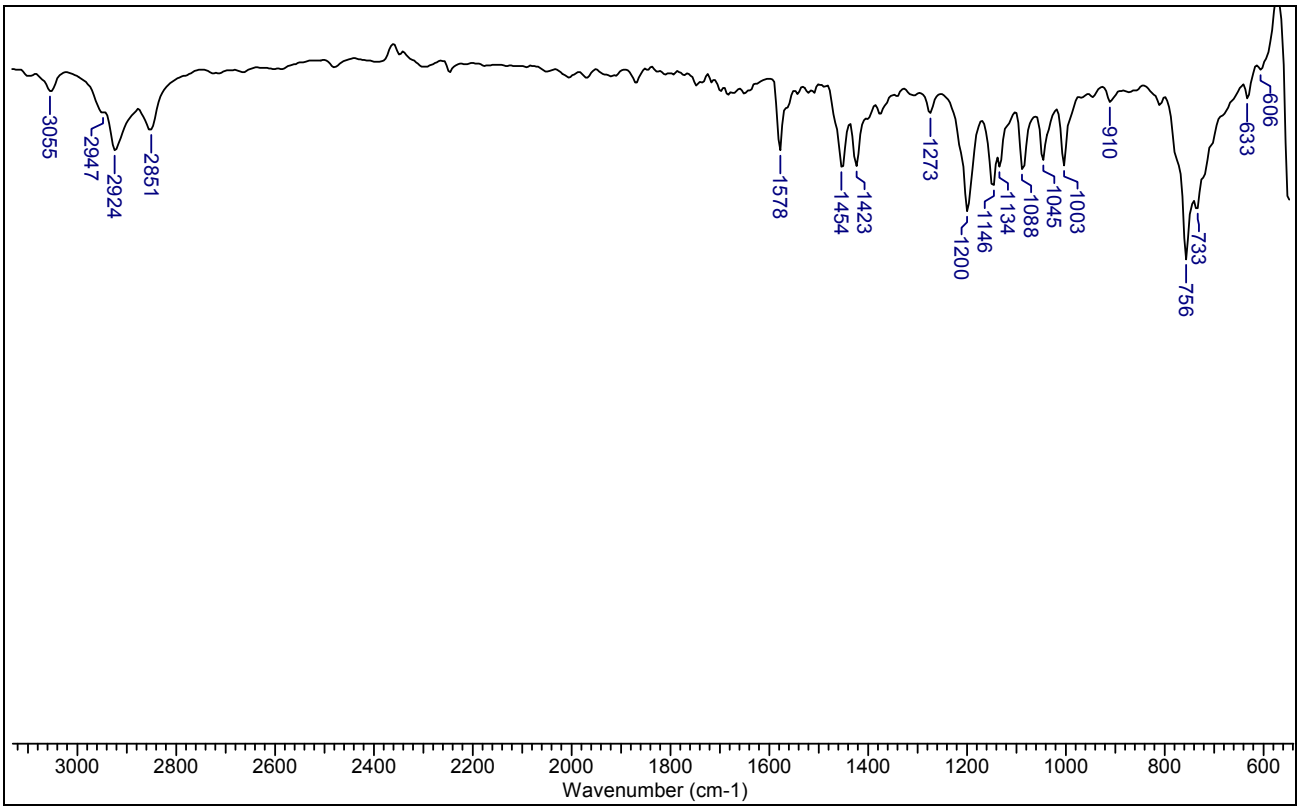

Figure S6. FT-IR spectrum of **{$Cu_2I_2[Py_2(PhCH_2)P{=}O]_2$}** (**4**).

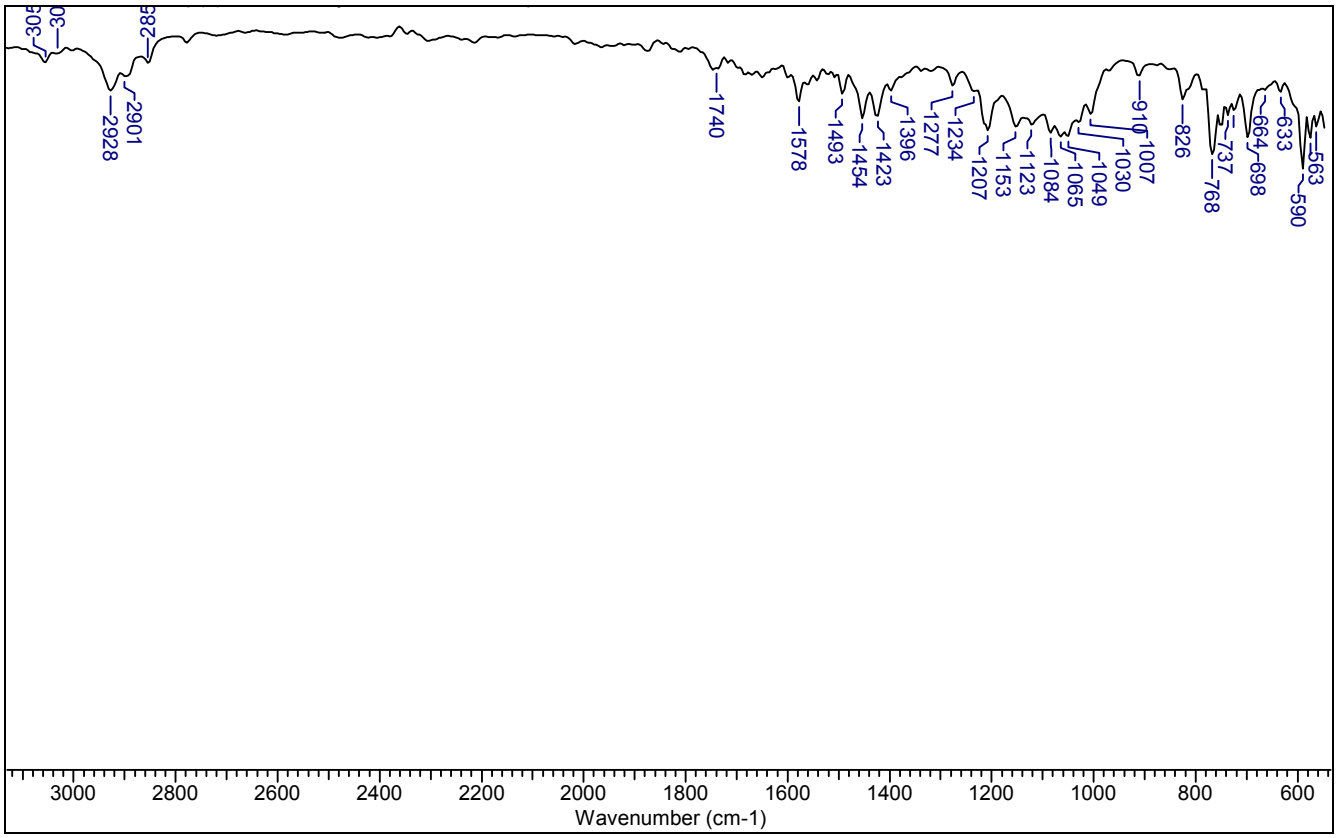

Figure S7. FT-IR spectrum of **{$Cu_2I_2[Py_2(1\text{-}NpCH_2)P{=}O]_2$}** (**5**).

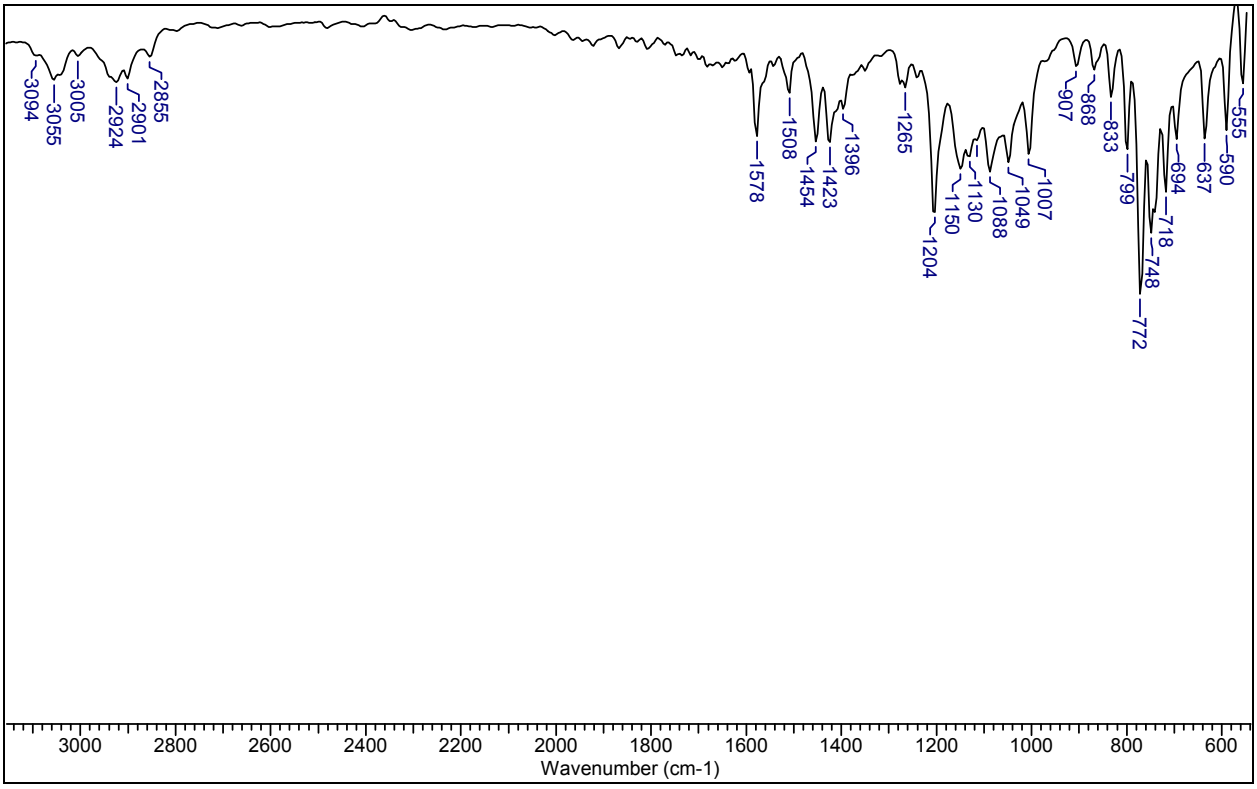

Figure S8. FT-IR spectrum of **{$Cu_2(SCN)_2[Py_2(Me)P{=}O]_2$}** (**6**).

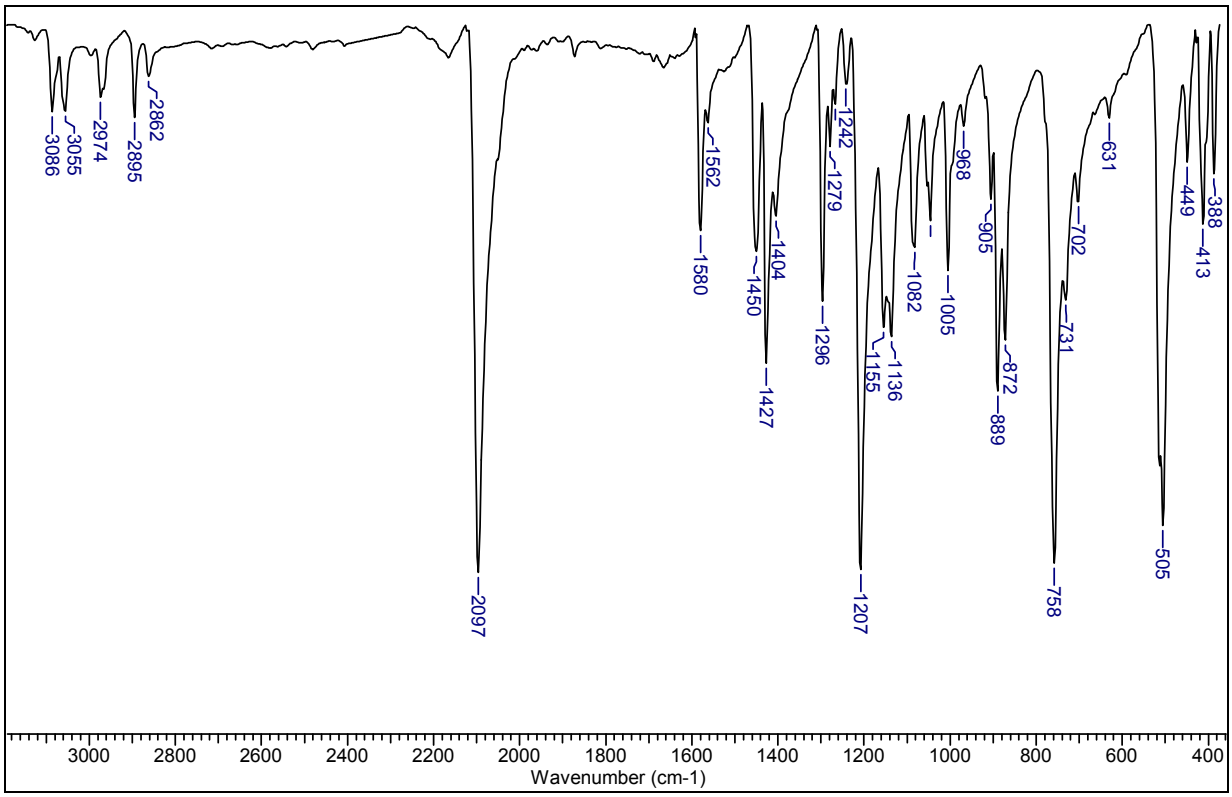

Figure S9. FT-IR spectrum of **{$Cu_2(SCN)_2[Py_2(Bu)P{=}O]_2$}** (**7**).

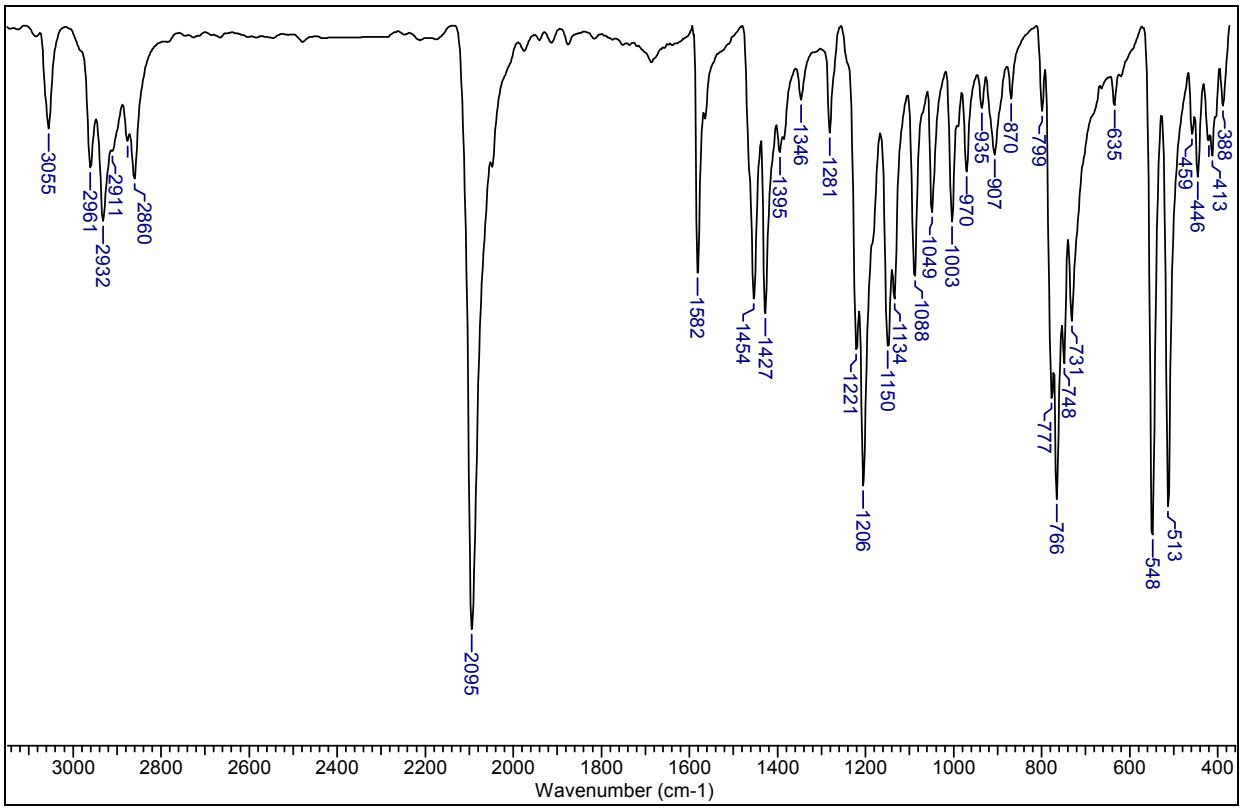

Figure S10. FT-IR spectrum of **{$Cu_2(SCN)_2[Py_2(PhCH_2)P{=}O]_2$}** (**8**)

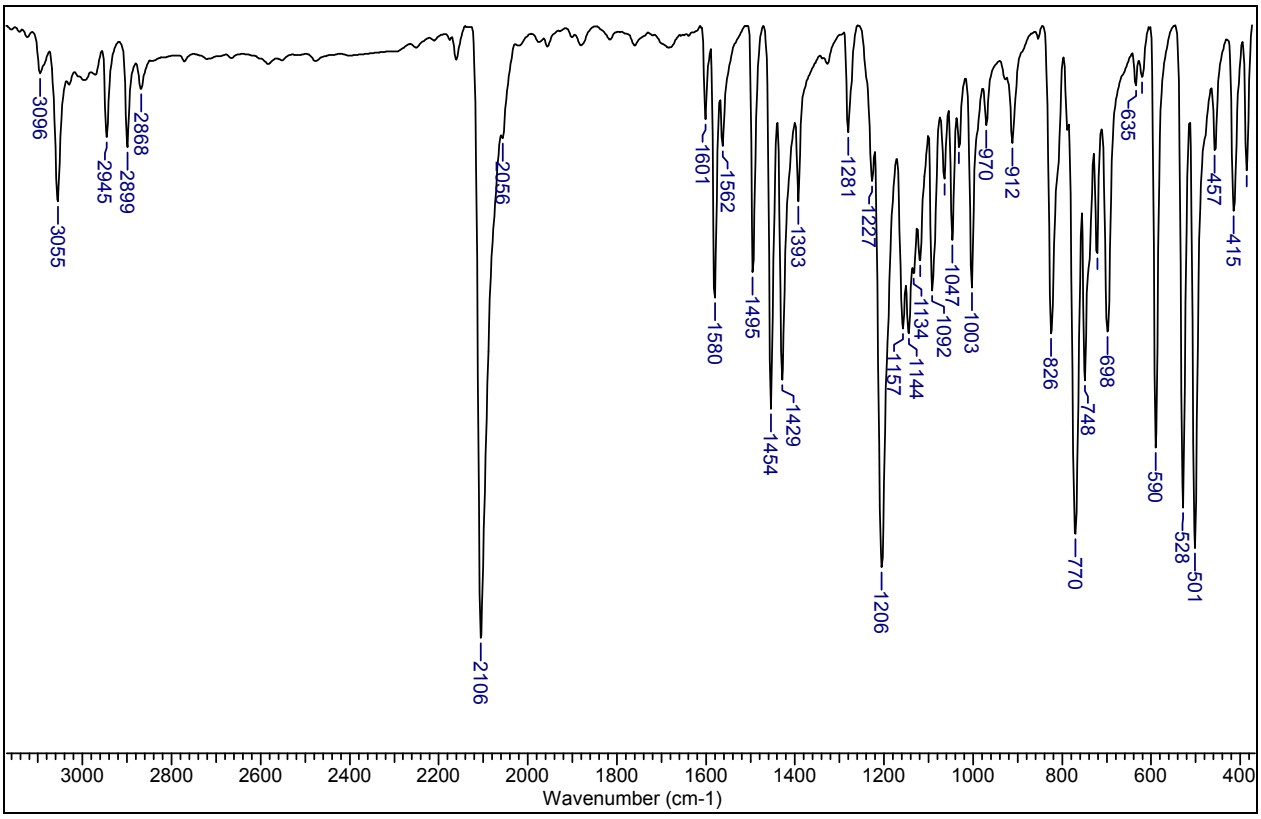

ESI-MS spectra of 1, 3 and 5

Figure S11. ESI-Mass spectra of **1** in positive- (***a***) and negative-ion (***b***) modes (MeCN).

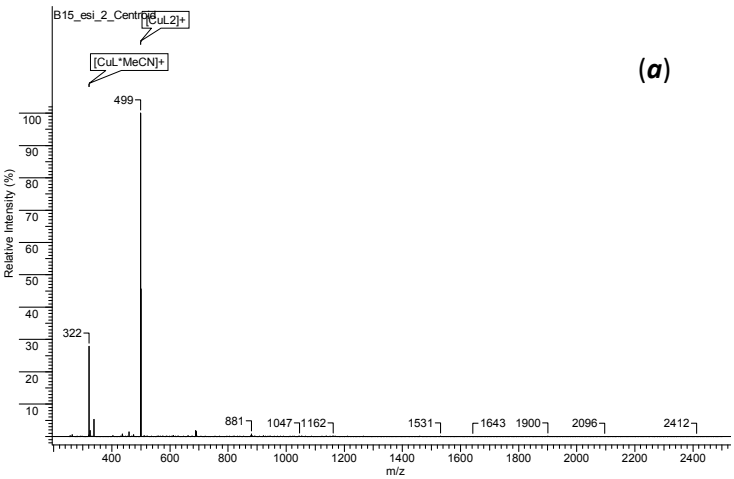

(***a***)

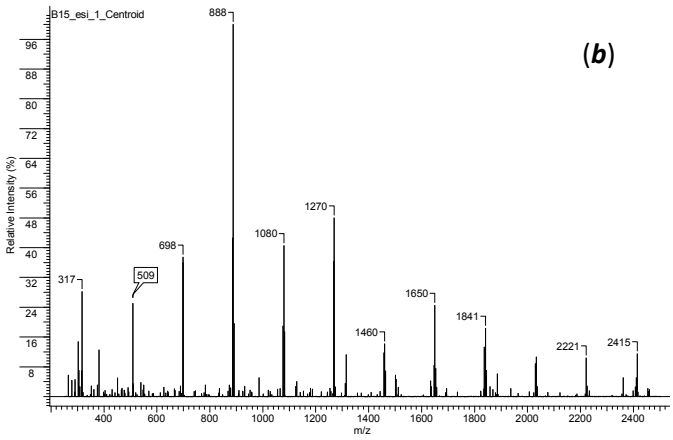

(***b***)

Figure S12. ESI-Mass spectra of **3** in positive- (***a***) and negative-ion (***b***) modes (MeCN).

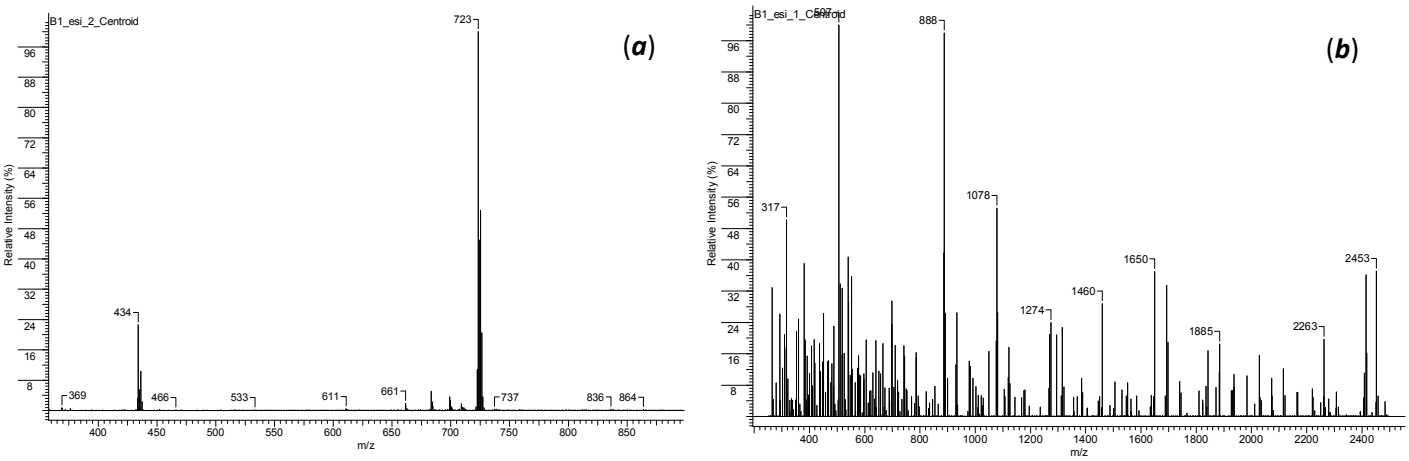

Figure S13. ESI-Mass spectra of **5** in positive- (***a***) and negative-ion (***b***) modes (MeCN).

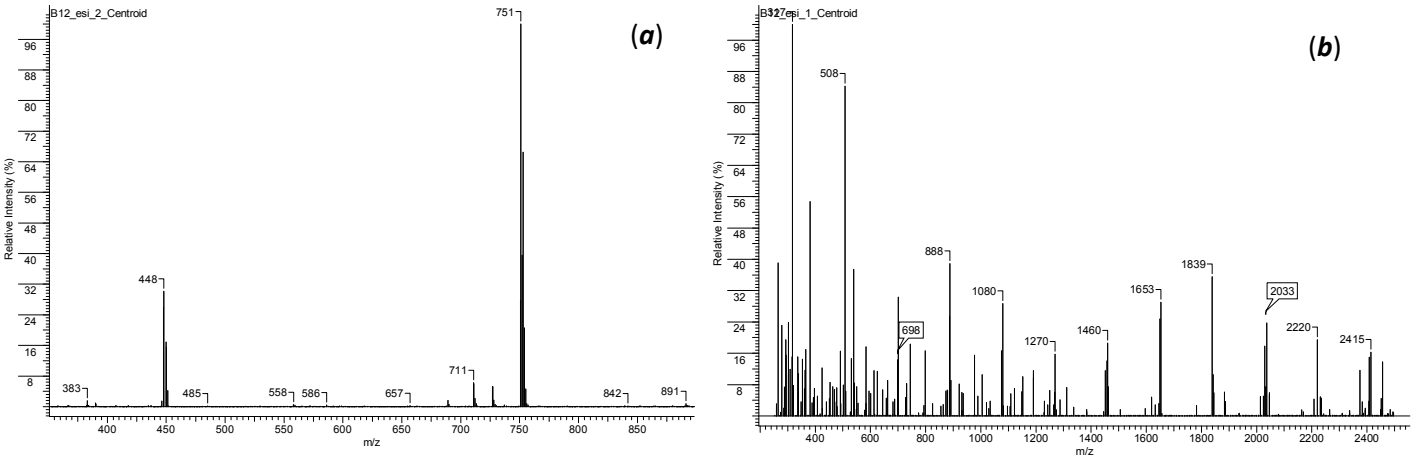

V.T. ^{31}P NMR spectra of 5

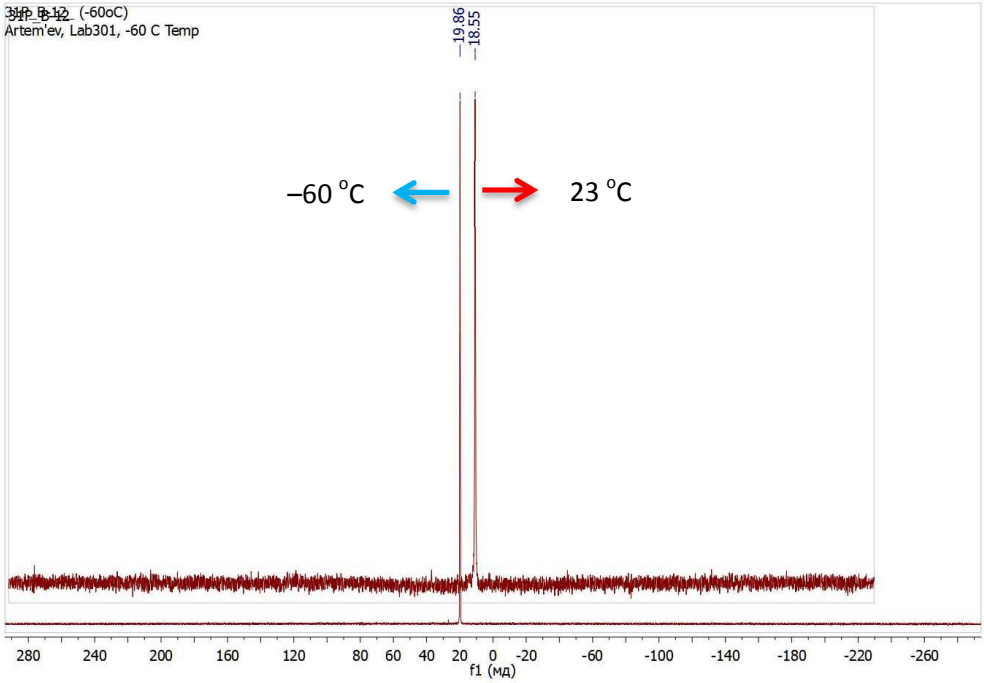

Figure S14. $^{31}P\{^{1}H\}$ NMR spectra of **5** measured at 23 and –60 °C in $CDCl_3$ solution.

Photophysical data

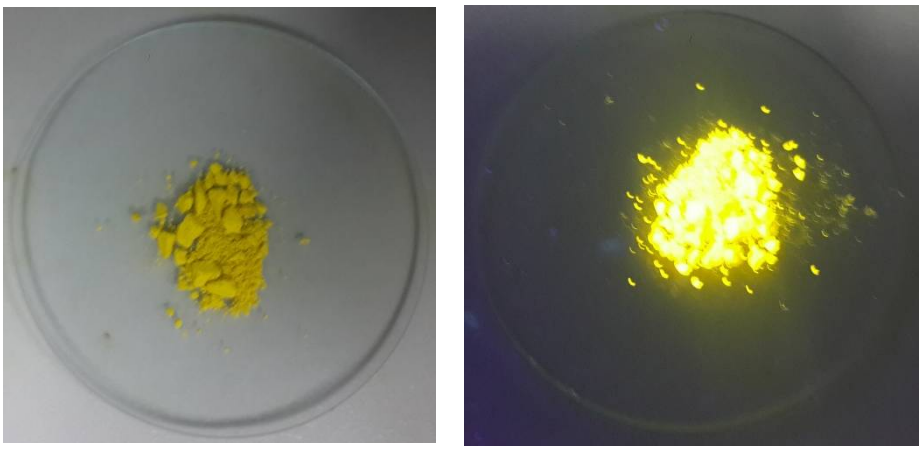

Figure S15. Photographs of the powder **1** under ambient light (*left*) and UV-light (*right*).

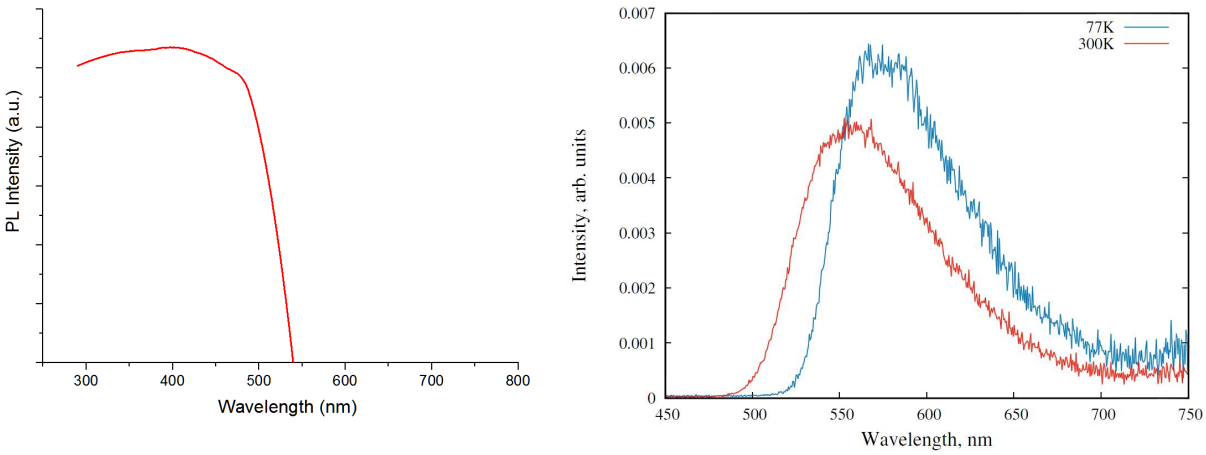

Figure S16. Excitation (at 300 K) and emission spectra (λ_{ex} = 400 nm) of **1** in the solid state at 77 and 300 K.

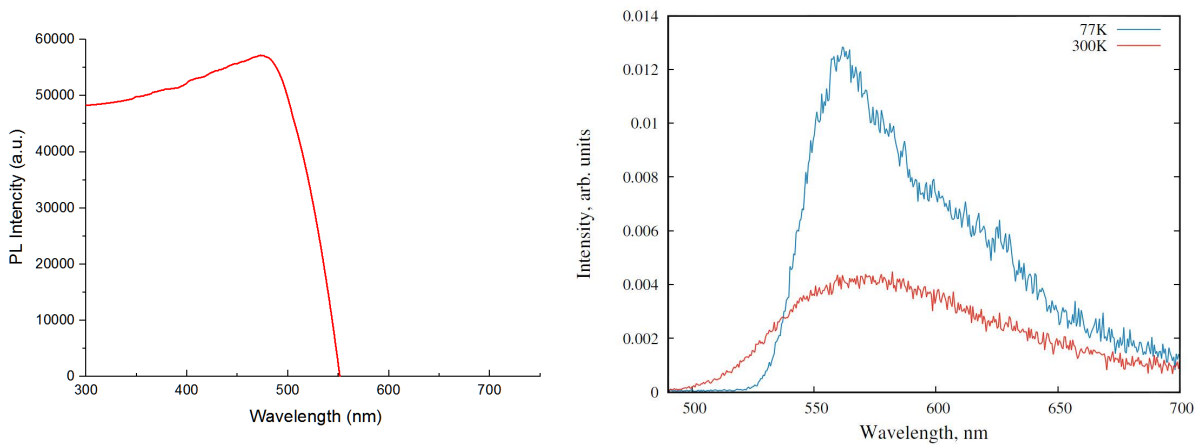

Figure S17. Excitation (at 300 K) and emission spectra (λ_{ex} = 470 nm) of **2** in the solid state at 77 and 300 K.

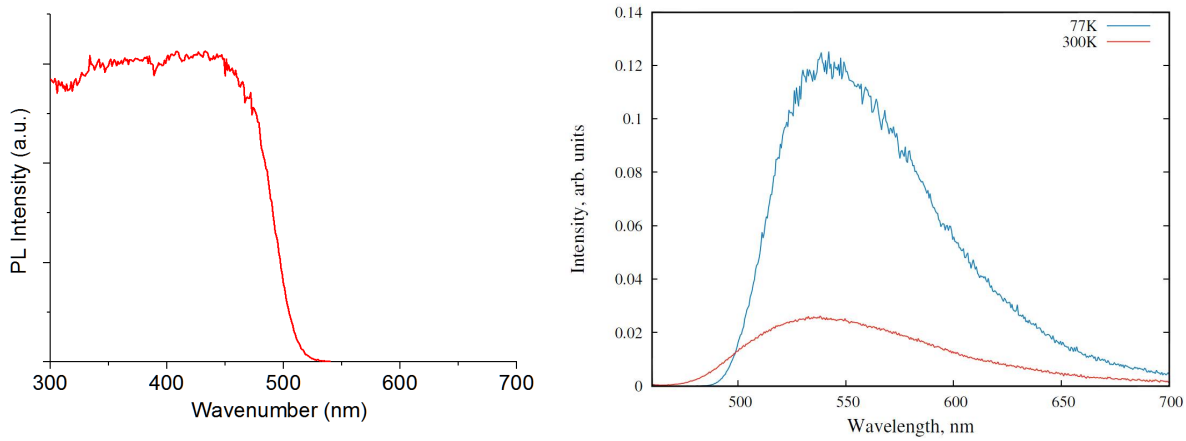

Figure S18. Excitation (at 300 K) and emission spectra (λ_{ex} = 450 nm) of **3** in the solid state at 77 and 300 K.

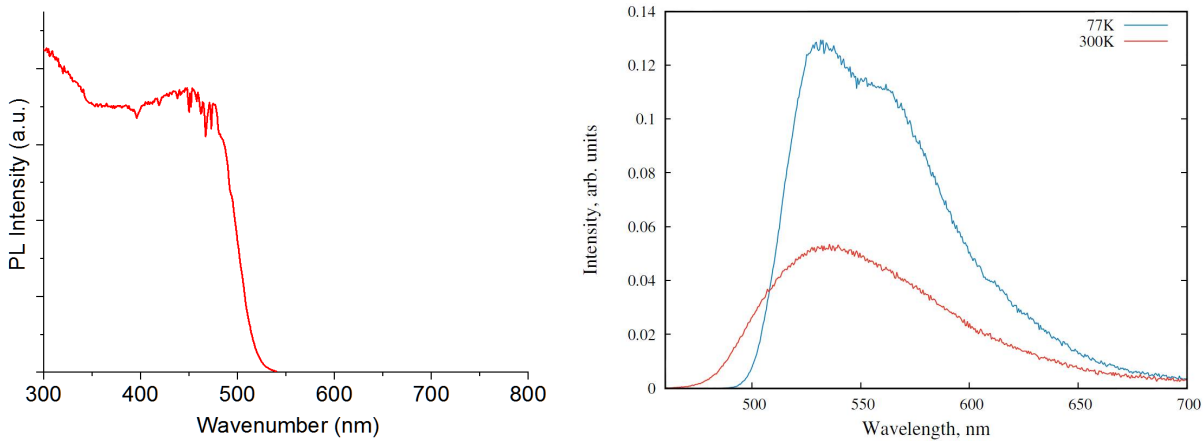

Figure S19. Excitation (at 300 K) and emission spectra (λ_{ex} = 450 nm) of **4** in the solid state at 77 and 300 K.

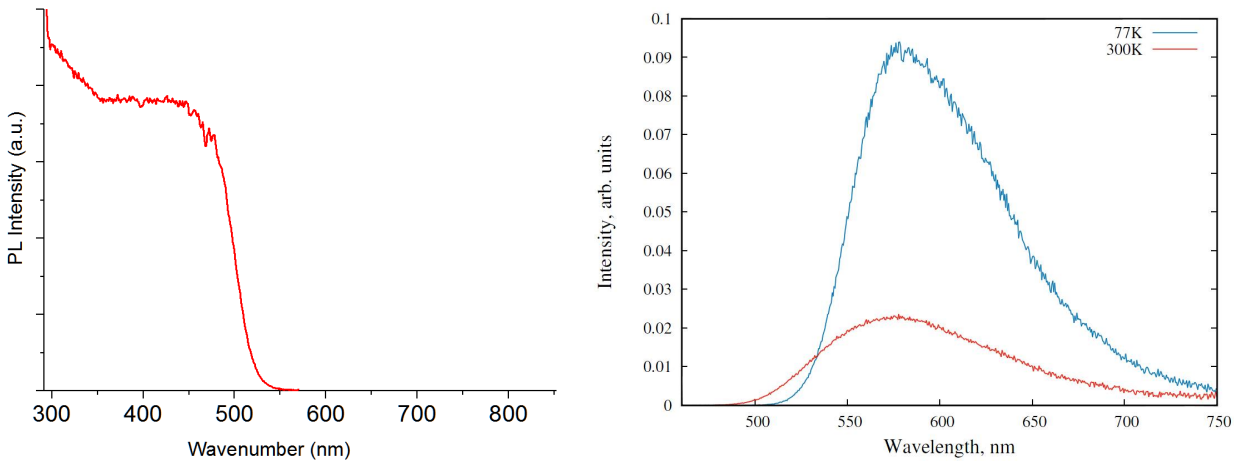

Figure S20. Excitation (at 300 K) and emission spectra (λ_{ex} = 450 nm) of **5** in the solid state at 77 and 300 K.

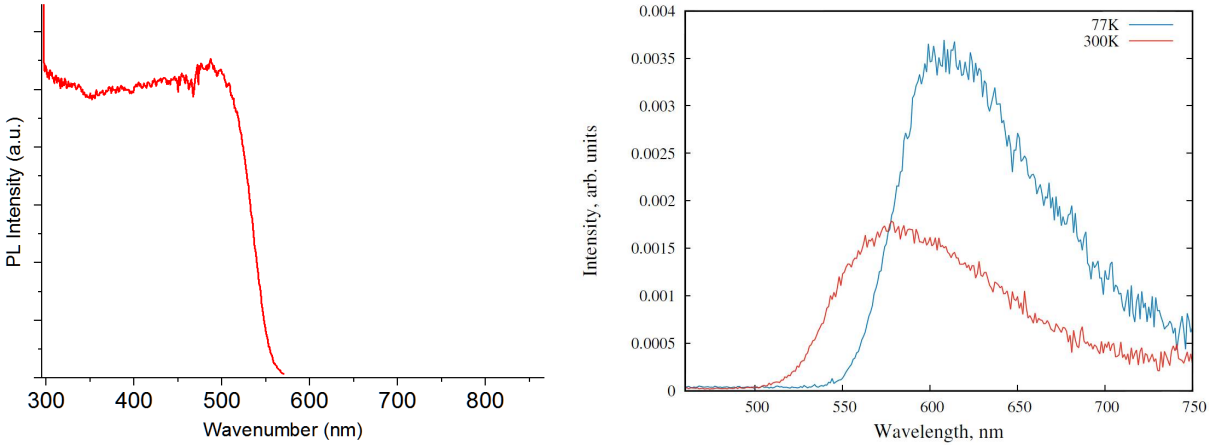

Figure S21. Excitation (at 300 K) and emission spectra (λ_{ex} = 400 nm) of **6** in the solid state at 77 and 300 K.

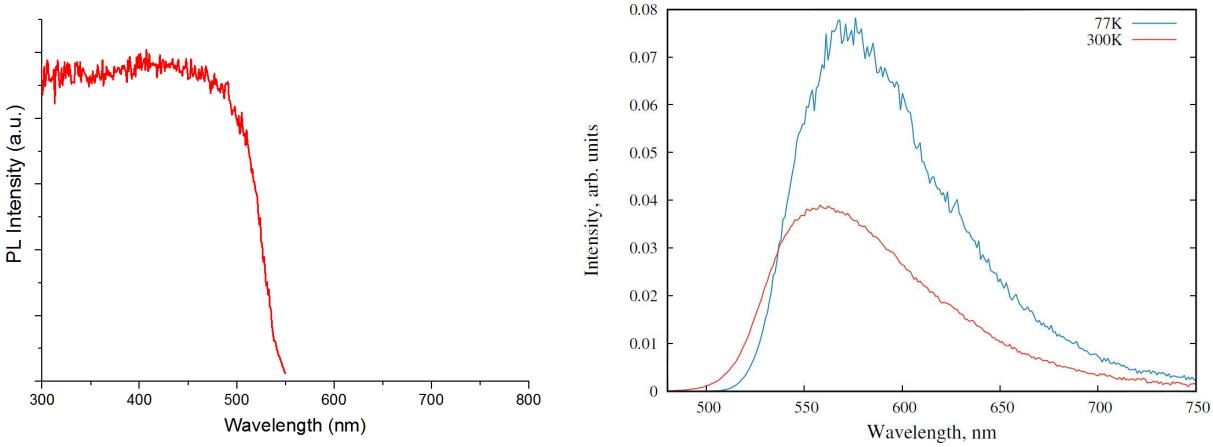

Figure S22. Excitation (at 300 K) and emission spectra (λ_{ex} = 480 nm) of **7** in the solid state at 77 and 300 K.

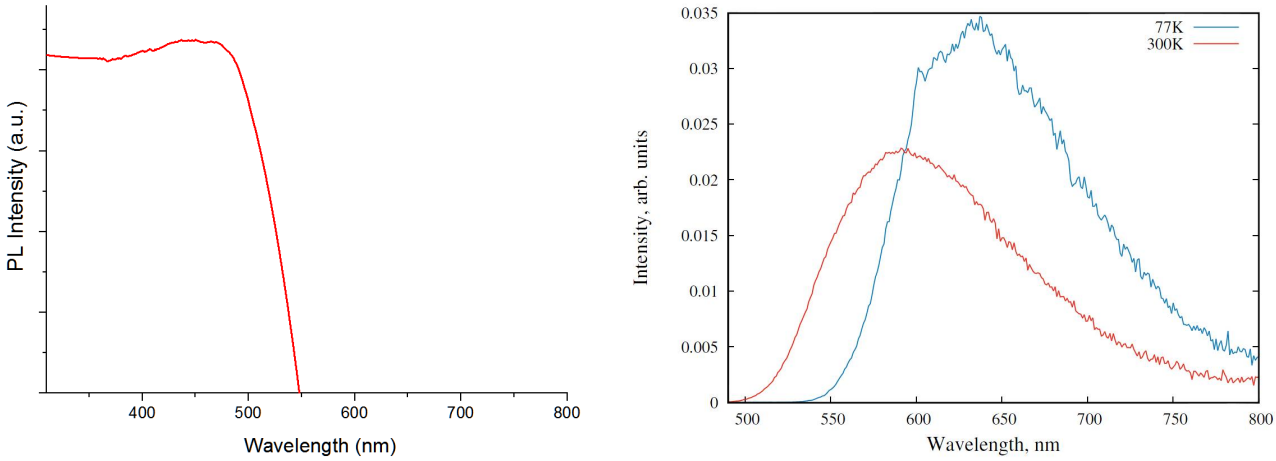

Figure S23. Excitation (at 300 K) and emission spectra (λ_{ex} = 450 nm) of **8** in the solid state at 77 and 300 K.

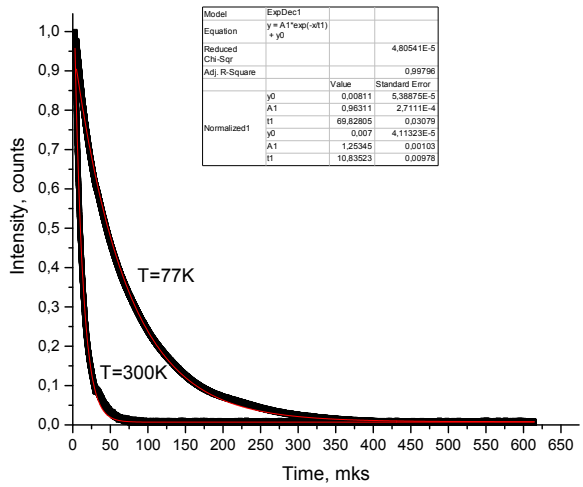

Figure S24. Emission decays for complex **1** in the solid state at 77 K and 300 K (λ_{em} = 560 nm, λ_{ex} = 355 nm).

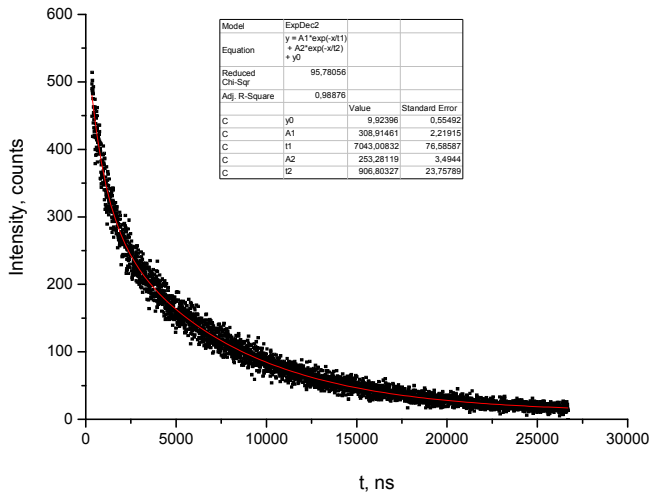

Figure S25. Emission decays for complex **2** in the solid state at 300 K (λ_{em} = 575 nm, λ_{ex} = 470 nm).

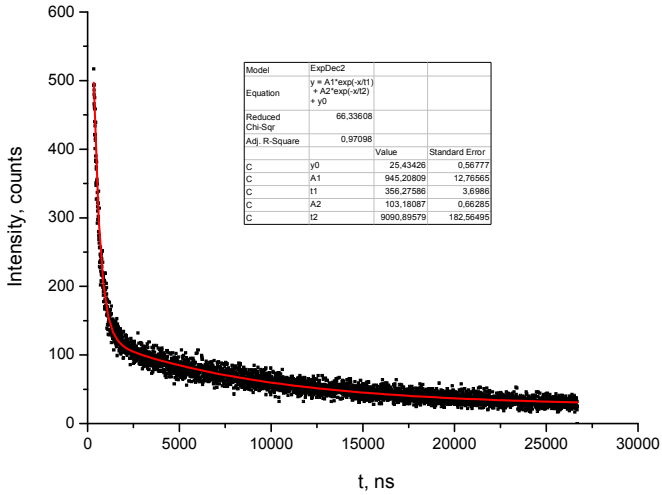

Figure S26. Emission decays for complex **3** in the solid state at 300 K (λ_{em} = 537 nm, λ_{ex} = 450 nm).

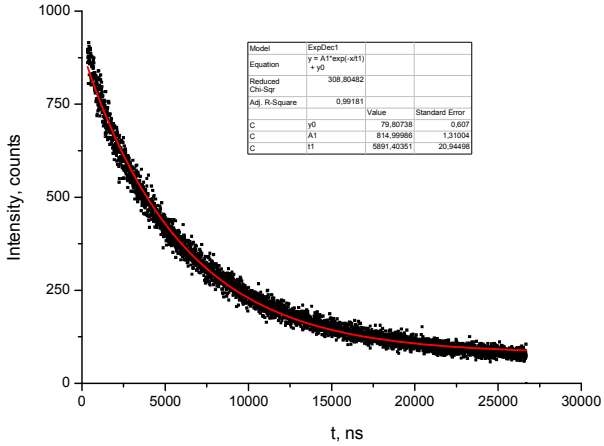

Figure S27. Emission decays for complex **4** in the solid state at 300 K (λ_{em} = 536 nm, λ_{ex} = 450 nm).

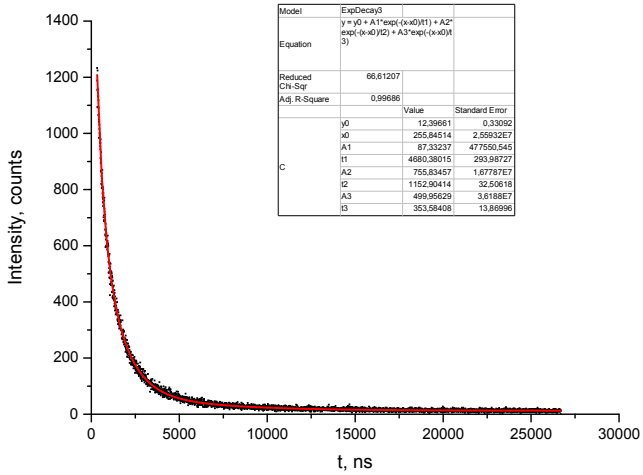

Figure S28. Emission decays for complex **5** in the solid state at 300 K (λ_{em} = 536 nm, λ_{ex} = 450 nm).

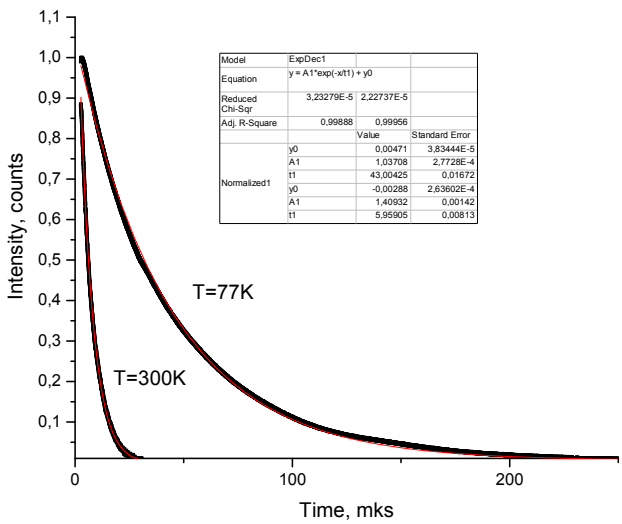

Figure S29. Emission decays for complex **6** in the solid state at 77 K and 300 K (λ_{em} = 580 nm, λ_{ex} = 355 nm).

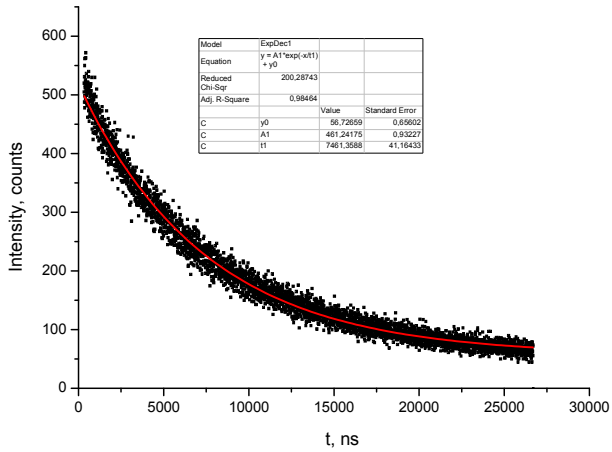

Figure S30. Emission decays for complex **7** in the solid state at 300 K (λ_{em} = 560 nm, λ_{ex} = 480 nm).

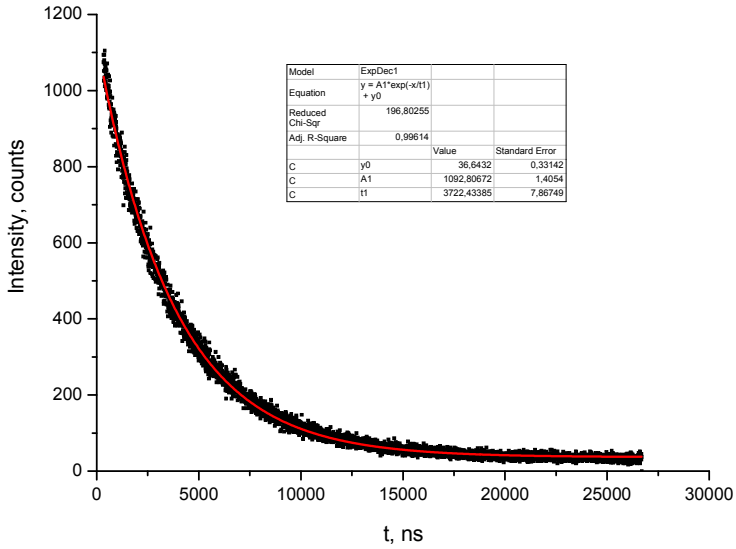

Figure S31. Emission decays for complex **8** in the solid state at 300 K (λ_{em} = 592 nm, λ_{ex} = 450 nm).

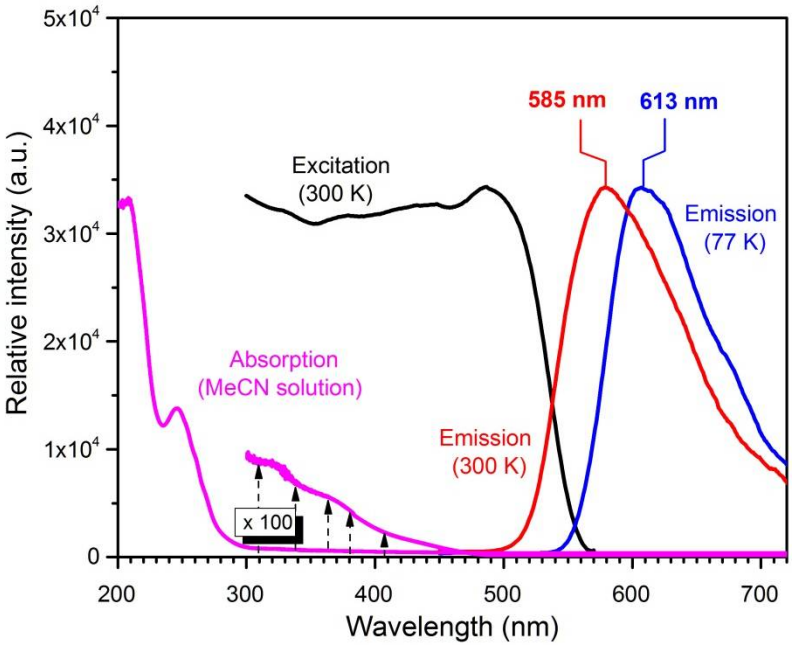

Figure S32. Absorption, excitation and emission (**λ**$_{ex}$ = 400 mn) spectra of **6**. The absorption spectrum is recorded for a MeCN solution, while excitation and emission spectra are given for a powder of **6**.

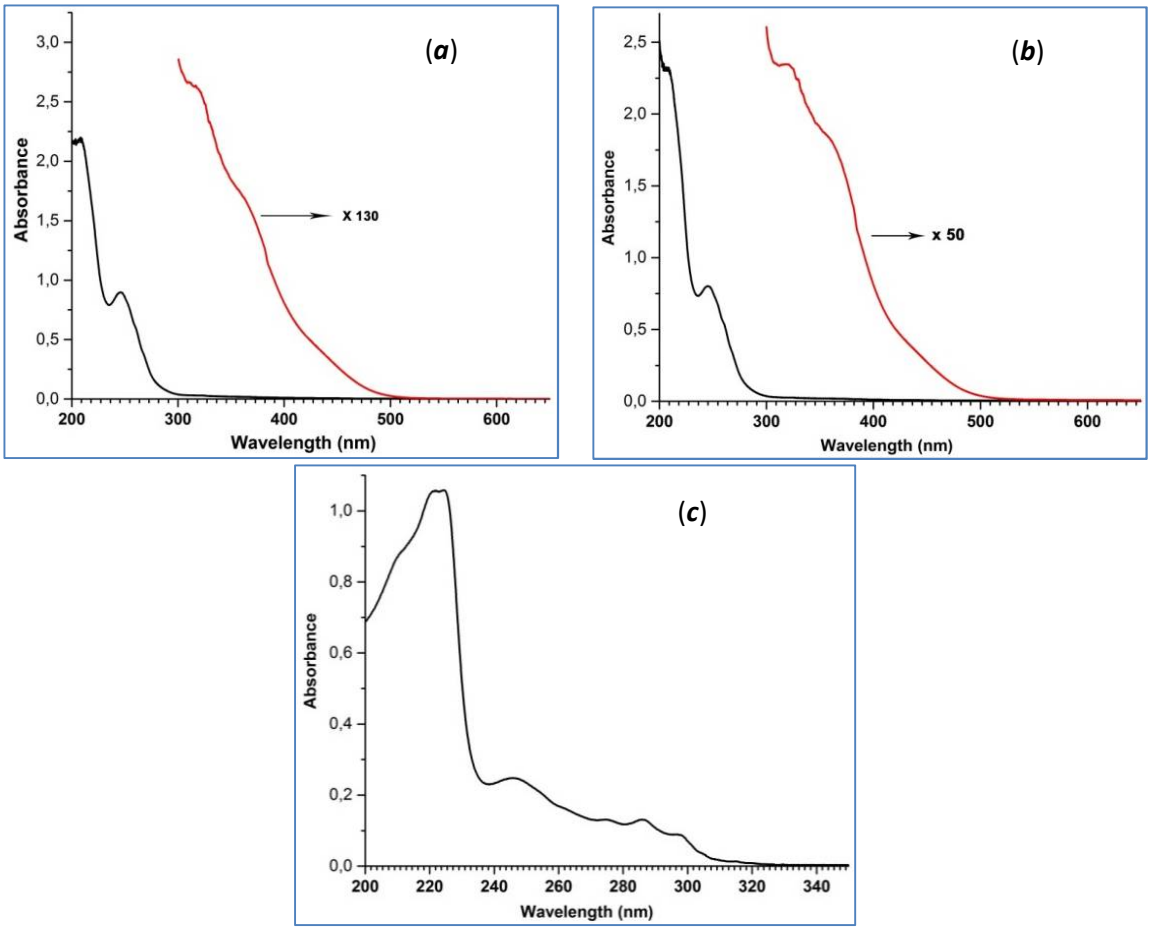

Figure S33. Absorption spectra of **3** (*a*), **4** (*b*) and **5** (*c*) measured for MeCN solution.

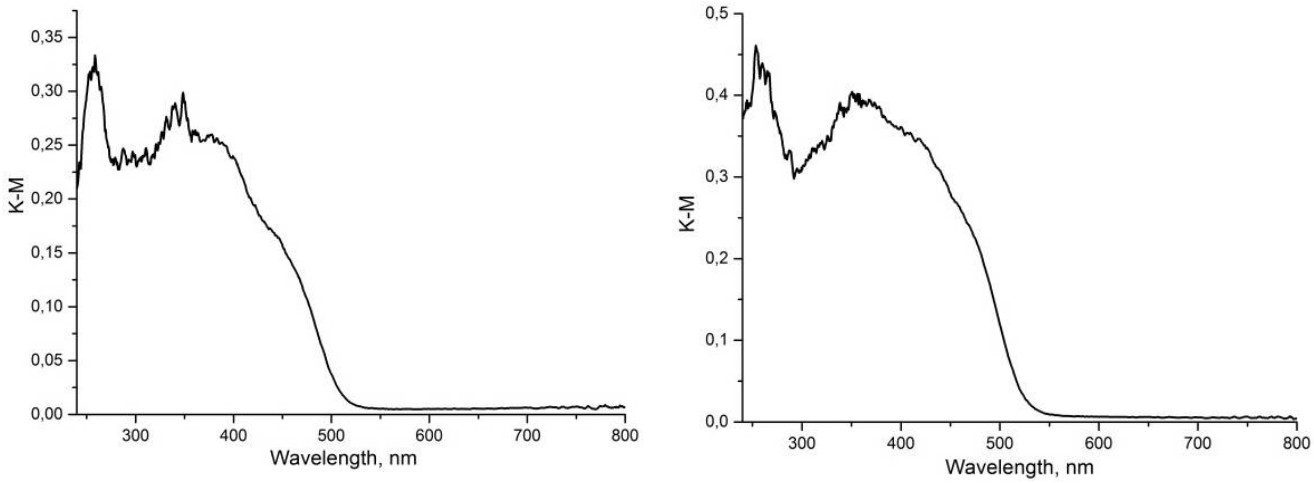

Figure S34. The solid-state UV–Vis absorption spectra of **1** (*left*) and **6** (*right*).

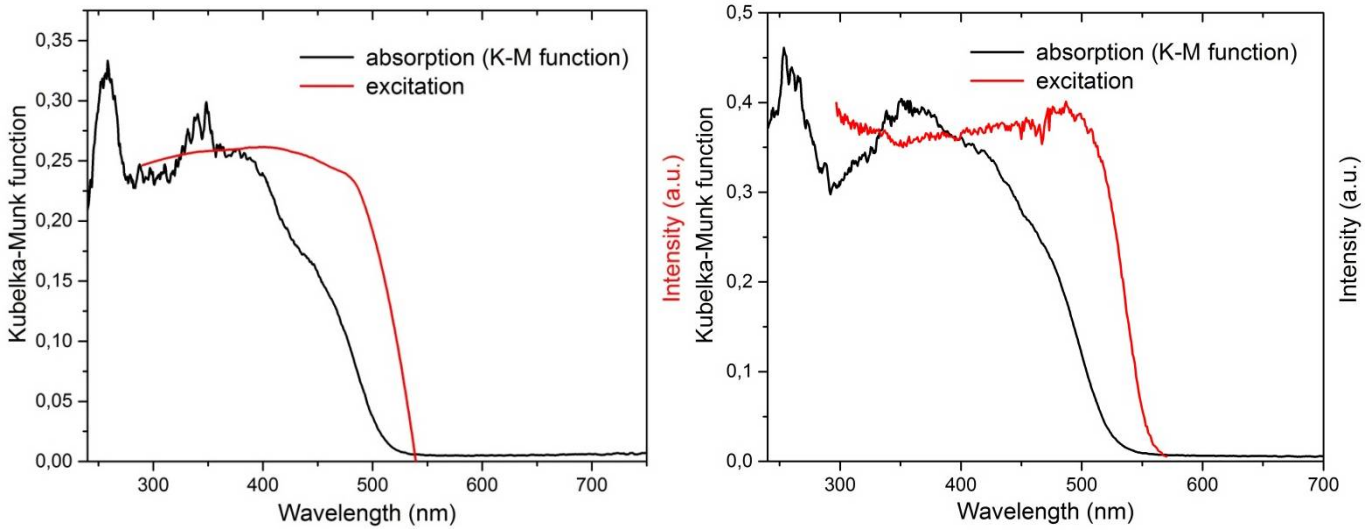

Figure S35. Comparison of excitation and solid-state UV–Vis absorption spectra for **1** (*left*) and **6** (*right*).

Computation details

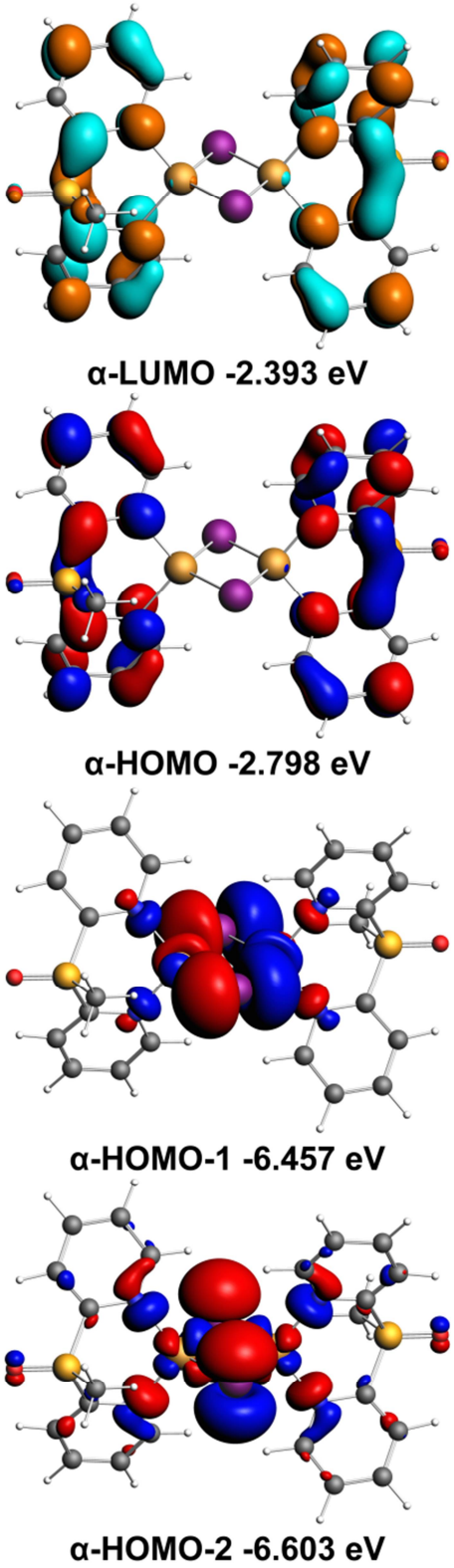

Figure S36. Near Fermi level molecular orbitals for T_1 state of complex **1**-C_i.

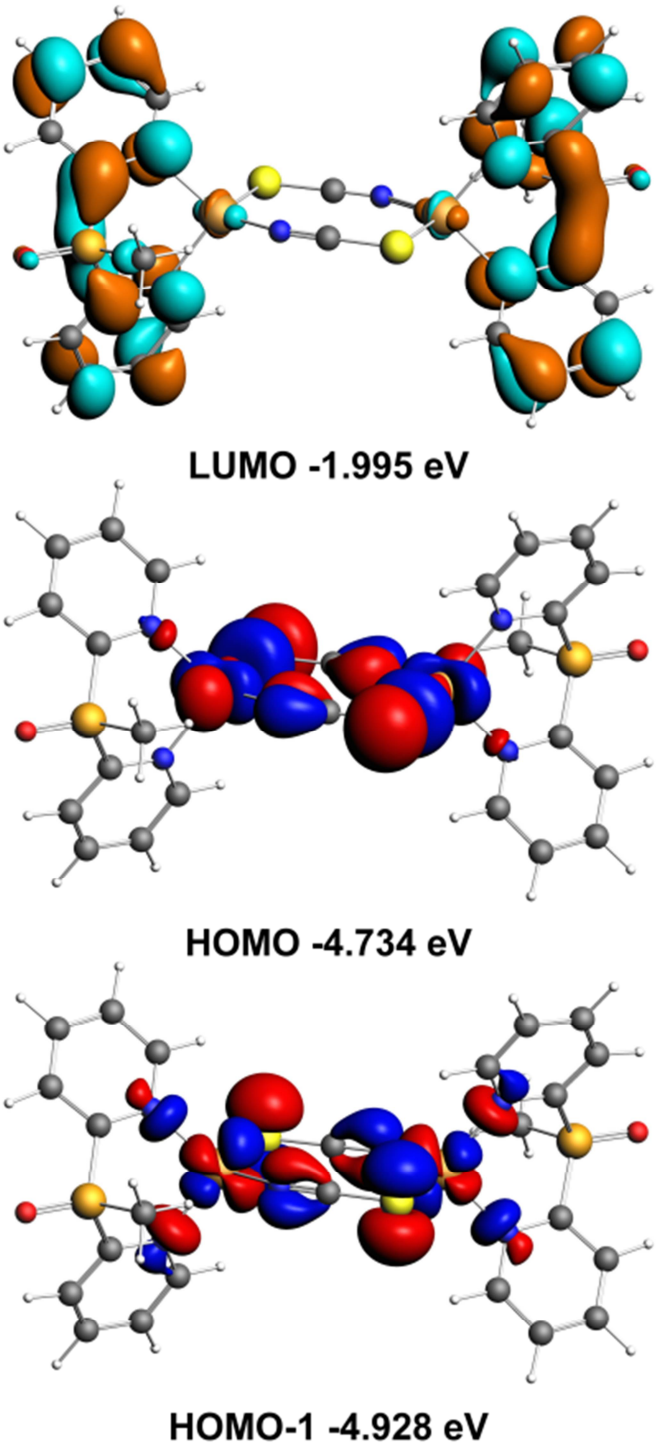

Figure S37. Near Fermi level molecular orbitals for S_0 state of complex **6**.

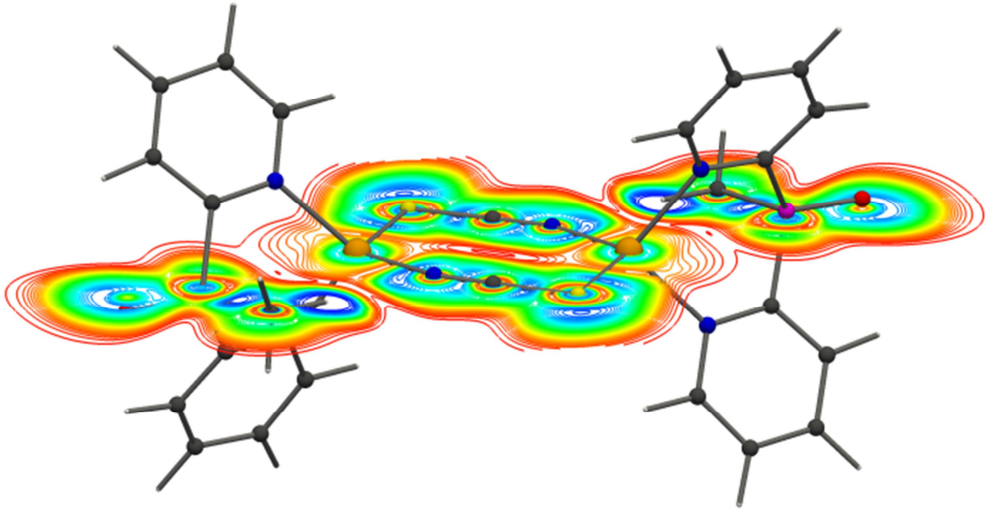

Figure S38. ELF map for S_0 state of complex **6**.

Table S3. Selected optimized and experimental geometrical parameters for complex **6** and calculated energetic parameters for its different states. E (kcal/mol) is formation energy, ΔE (kcal/mol) is energy difference between ground state (S_0) and exited states (S_1 and T_1), $D_{Cu–Cu}$ (Å), $D_{Cu–N}$ (Å), $D_{Cu–S}$ (Å) and $D_{C–N}$ (Å) are Cu–Cu, Cu–N, Cu–S and C–N distances, α (°) is N–Cu–S angle.

Structure	E	ΔE	$D_{Cu–Cu}$	$D_{Cu–N}$	$D_{Cu–S}$	$D_{C–N}$	α N–Cu–S
6 S_0	-10208.46	0	5.026	1.932	2.394	1.165	109.4
6 S_1	-10166.17	42.29	5.267	1.929	2.403	1.163	99.1
6 T_1	-10166.41	42.05	5.189	1.928	2.402	1.164	100.5
X-ray structure **6** (Fig. 4)	n/a	n/a	5.103	1.952	2.391	1.148	105.7

TGA/DTA curves for 1 and 6

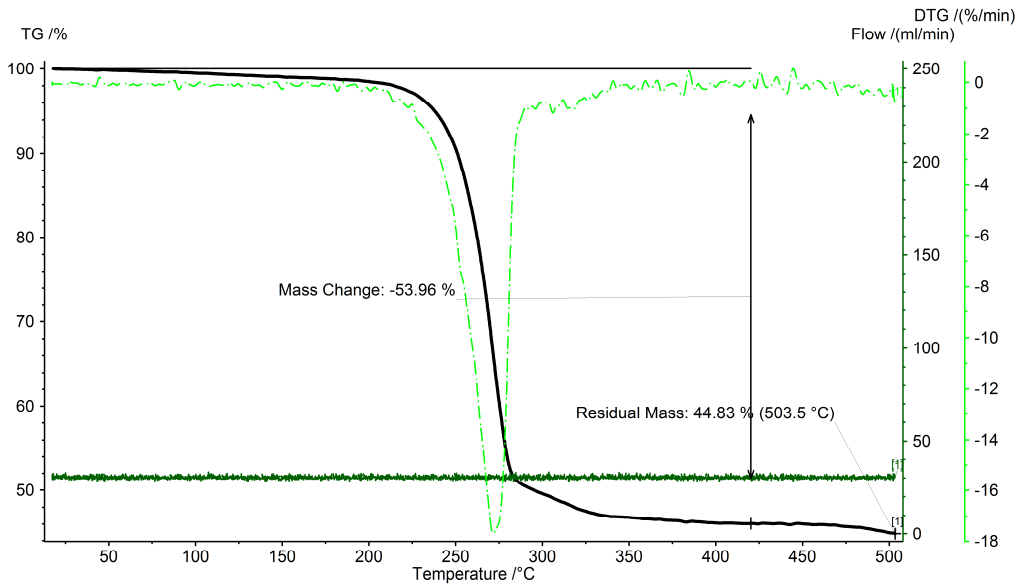

Figure S39. The TGA/DTA curves for **1**.

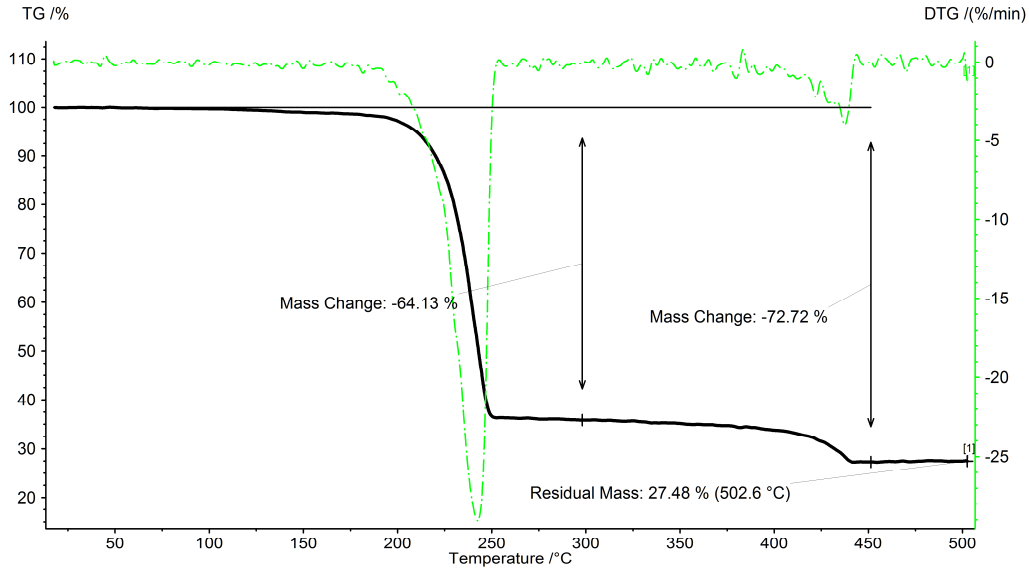

Figure S40. The TGA/DTA curves for **6**.